University of Windsor
Leddy Library

Article

Chirality Dependent Potency Enhancement and Structural Impact of Glycol Nucleic Acid Modification on siRNA

Mark K Schlegel, Donald J. Foster, Alexander V Kel'in, Ivan Zlatev, Anna Bisbe, Muthusamy Jayaraman, Jeremy G. Lackey, Kallanthottathil G Rajeev, Klaus Charisse, Joel Harp, Pradeep S. Pallan, Martin A. Maier, Martin Egli, and Muthiah Manoharan

ACS Publications

1
2
3
4
5
6
7
8
9
10
11
12
13
14
15
16
17
18
19
20
21
22
23
24
25
26
27
28
29
30
31
32
33
34
35
36
37
38
39
40
41
42
43
44
45
46
47
48
49
50
51
52
53
54
55
56
57
58
59
60

Chirality Dependent Potency Enhancement and Structural Impact of Glycol Nucleic Acid Modification on siRNA

Mark K. Schlegel[1]*, Donald J. Foster[1], Alexander V. Kel'in[1], Ivan Zlatev[1], Anna Bisbe[1], Muthusamy Jayaraman[1], Jeremy G. Lackey[1#], Kallanthottathil G. Rajeev[1], Klaus Charissé[1], Joel Harp[2], Pradeep S. Pallan[2], Martin A. Maier[1], Martin Egli[2] and Muthiah Manoharan[1]*

[1]*Alnylam Pharmaceuticals, 300 Third Street, Cambridge, Massachusetts 02142*
[2]*Vanderbilt University School of Medicine, Department of Biochemistry, Nashville, Tennessee 37232*
[#]*present address: Quantum-Si Inc, 530 Old Whitfield Street, Guilford, Connecticut, 06437*

Abstract

Here we report the investigation of glycol nucleic acid (GNA), an acyclic nucleic acid analog, as a modification of siRNA duplexes. We evaluated the impact of (*S*)- or (*R*)-GNA nucleotide incorporation on RNA duplex structure by determining three individual crystal structures. These structures indicate that the (*S*)-nucleotide backbone adopts a conformation that has little impact on the overall duplex structure, while the (*R*)-nucleotide disrupts the phosphate backbone and hydrogen bonding of an adjacent base pair. In addition, the GNA-T nucleobase adopts a rotated conformation in which the 5-methyl group points into the minor groove, rather than the major groove in a normal Watson-Crick base pair. This observation of reverse Watson-Crick base pairing is further supported by thermal melting analysis of GNA-C and GNA-G containing duplexes where it was demonstrated that a higher thermal stability was associated with isoguanine and isocytosine base pairing, respectively, over the canonical nucleobases. Furthermore, it was also shown that GNA nucleotide or dinucleotide incorporation increases resistance against snake venom phosphodiesterase. Consistent with the structural data, modification of an siRNA with (*S*)-GNA resulted in greater *in vitro* potencies over identical sequences containing (*R*)-GNA. A walk of (*S*)-GNA along the guide and passenger strands of a conjugate duplex targeting mouse transthyretin (TTR) indicated that GNA is well tolerated in the seed region of both strands *in vitro*, resulting in an approximate 2-fold improvement in potency. Finally, these conjugate duplexes modified with GNA were capable of maintaining *in vivo* potency when subcutaneously injected into mice.

Introduction

RNA interference (RNAi) is the endogenous biological process through which double-stranded small interfering RNA (siRNA) mediates sequence-specific gene silencing of target mRNA.[1-4] Recognition of the intended mRNA target is accomplished after the siRNA duplex is recognized and bound by the endonuclease protein Argonaute 2 (Ago2), the catalytic component within the RNA-induced silencing complex (RISC). Once bound, the passenger strand (also referred to as the sense strand) is specifically cleaved between positions 10 and 11 and subsequently dissociates from RISC.[3-5] The guide strand (also referred to as the antisense strand) remains in the active RISC complex whereupon it can recognize and cleave the target mRNA. While exogenous synthetic siRNAs also have the capability to induce gene-silencing via the endogenous RNAi pathway, they must include various chemical modifications in order to stabilize these molecules against nuclease degradation, reduce their immunostimulatory potential, and facilitate their uptake into cells.[6] For example, strategically placed 2'-ribose modifications and conjugation to a targeting tri-N-acetylgalactosamine (GalNAc) ligand, specifically recognized by the asialoglycoprotein receptor, have resulted in siRNAs which are currently being evaluated in pre-clinical and clinical studies for therapeutic silencing of genes in hepatocytes.[7-10]

With regards to chemical modifications of siRNAs, it has been demonstrated that acyclic, thermally destabilizing modifications have the capability to improve stability and/or enhance RNAi-mediated gene silencing via several different mechanisms.[11-14] For instance, differentiation between the two strands of an siRNA that is loaded within Argonaute strongly depends on the thermal stability of the terminal regions of the duplex; Ago2 favors loading of the 5'-end of the strand from the duplex end which has a lower thermal stability.[15-18] It has been shown that thermally destabilizing modifications incorporated at certain positions of an siRNA duplex can lead to an increase in potency by improving strand bias, thereby favoring loading of the desired guide strand into RISC. In addition, the introduction of thermally destabilizing modifications may help facilitate sense strand dissociation during Ago2 loading, thereby increasing the rate of formation of active RISC.[3]

Along these lines, we wanted to investigate the potential of glycol nucleic acid (GNA) as a modification within siRNA (Figure 1). Previous work has demonstrated that the (*S*)-isomer of GNA, comprised of a flexible acyclic, three-carbon backbone with only one stereocenter,

crosspairs with RNA in an A/T rich context, whereas the (*R*)-isomer does not.[19,20] Analysis of the crystal structures of several GNA homoduplexes have shown that (*S*)-GNA forms a right-handed duplex with helical parameters that resemble the A-form, whereas (*R*)-GNA would presumably form a left-handed duplex.[21-23] Although it has been demonstrated that the incorporation of GNA nucleotides is thermally destabilizing in a DNA duplex[20], it is unclear as to what extent the incorporation of GNA affects the thermal and/or metabolic stability of an RNA duplex. Herein we report the impact of RNA nucleotide or base pair substitution using both stereoisomers of GNA on *in vitro* and *in vivo* siRNA potency, duplex thermal stability, resistance to degradation by snake venom phosphodiesterase (SVPD), and RNA duplex structure.
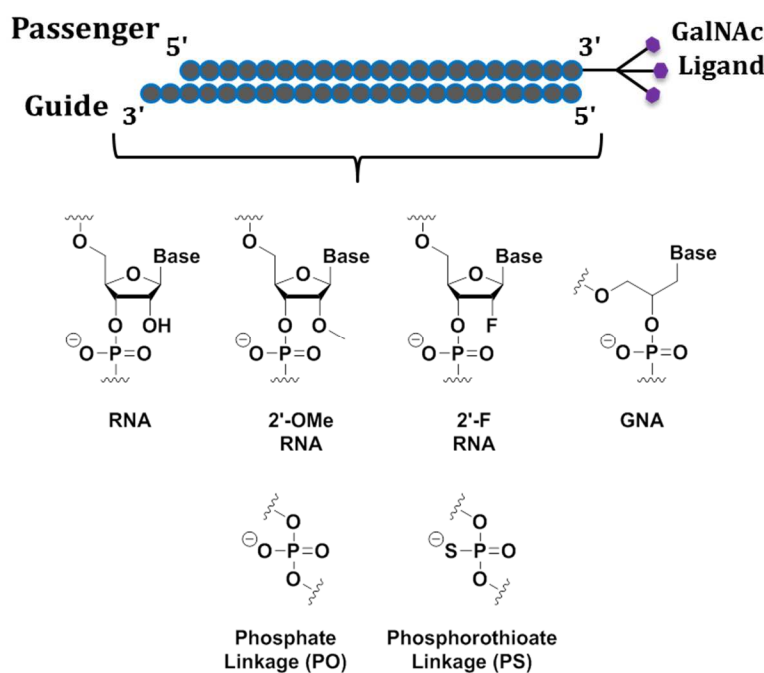
Figure 1. Structural overview of an siRNA-GalNAc conjugate duplex.[7] Also shown are the structures of the nucleotides used in this study, including 2'-*O*-methyl (2'-OMe), 2'-deoxy-2'-fluoro (2'-F), and GNA. Backbone modifications include both natural phosphate (PO) and phosphorothioate (PS) linkages.

Results

Thermal Stability of GNA/RNA Heteroduplexes. The impact of GNA incorporation on RNA duplex thermal stability was measured in a series of 12-mer RNA duplexes. Single

substitution of an RNA nucleotide with GNA resulted in an average destabilization of 10.3 °C and 11.6 °C for the (*S*)- and (*R*)-GNA isomers, respectively (Table 1). The difference in stability between the two isomers was specific to the identity of the nucleobase; substitution of an A, T, or C nucleotide resulted in more stable duplexes for the (*S*)-isomer compared to the (*R*)-isomer, whereas G nucleotide substitution with the (*R*)-isomer resulted in a slightly more stable duplex compared to the (*S*)-isomer (Table 1). In addition, the impact of GNA substitution on stability was much greater within the context of G and C nucleotides (from 12-18 °C) compared to A or T nucleotides (from 5-9 °C). These results are consistent with previous reports by Meggers and colleagues who observed a similar discrepancy between A:T and G:C base pairs within RNA:GNA heteroduplexes.[20] Replacement of a single RNA base pair with GNA indicated little difference between the two isomers in the A:T base pairs, but a clear preference for the (*S*)-isomer in a G:C base pair (Table 1) with a $\Delta\Delta T$m of 7.5 °C.

Table 1. Impact of GNA substitution on thermal stability of duplexes.

Sequence Context 5'-UACAG**UC**UAUGU-3' 3'-AUGUC**AG**AUACA-5'	ΔT_{m} (°C)	
	(*S*)-isomer	(*R*)-isomer
Single substitution	-10.3 ± 5.3	-11.6 ± 4.7
A	-7.7	-9.1
T	-4.7	-7.6
G	-12.1	-11.6
C	-16.8	-18.2
Base pair substitution	-17.7 ± 3.4	-21.0 ± 9.3
A:T	-15.3	-14.4
G:C	-20.1	-27.6

The underlined RNA nucleotides were substituted with the indicated GNA nucleotide or base pair. All values are the average of two independent measurements at a duplex concentration of 2 µM in 1x PBS buffer (10 mM Na/K phosphate buffer, pH 7.4, with 137 mM NaCl and 2.7 mM KCl). The values shown for single or base pair substitution represent the average destabilization across all four nucleotides or two base pairs, respectively.

Resistance to 3'-exonuclease Degradation. Previous reports have demonstrated that the incorporation of acyclic nucleotides at the 3'-end of DNA oligonucleotides can enhance resistance towards 3'-exonuclease degradation.[13] To assess the stability of GNA-modified single

stranded oligonucleotides towards 3'-exonucleases, a series of strands containing single or double GNA substitution at the 3'-end of dT_{20} were analyzed in the presence of snake venom phosphodiesterase (SVPD). These results were compared with that of a control containing a single phosphorothioate linkage (PS) at the 3'-end (half-life of 2.7 hours, Figure 2). The oligonucleotides containing a single (*S*)- or (*R*)-GNA nucleotide with a natural phosphodiester linkage (PO) at the 3'-end were more stable than the control (PS) with half-lives of 5.6 and 8.0 hours, respectively (Figure 2A). Interestingly, the replacement of the PO linkage with PS between the 3'-terminal nucleotides had a consistent negative impact on nuclease resistance resulting in half-lives of only 2.1 and 2.7 hours for the (*S*)- and (*R*)-isomer, respectively. When the GNA nucleotide was moved to the penultimate position from the 3'-end, nuclease resistance was diminished in an all phosphate (PO) context, but greatly enhanced in the presence of PS to 20.1 and 19.6 hours for the (*S*)- and (*R*)-isomer, respectively (Figure 2B). Finally, the substitution of both 3'-terminal nucleotides with GNA, connected through a PO linkage, resulted in roughly an 8- or 5-fold increase in nuclease resistance for the (*S*)- or (*R*)-isomer, respectively (Figure 2C). In contrast to the case of single substitution, the presence of a terminal PS linkage between the GNA-GNA dinucleotide had only a minor effect on resistance to degradation.
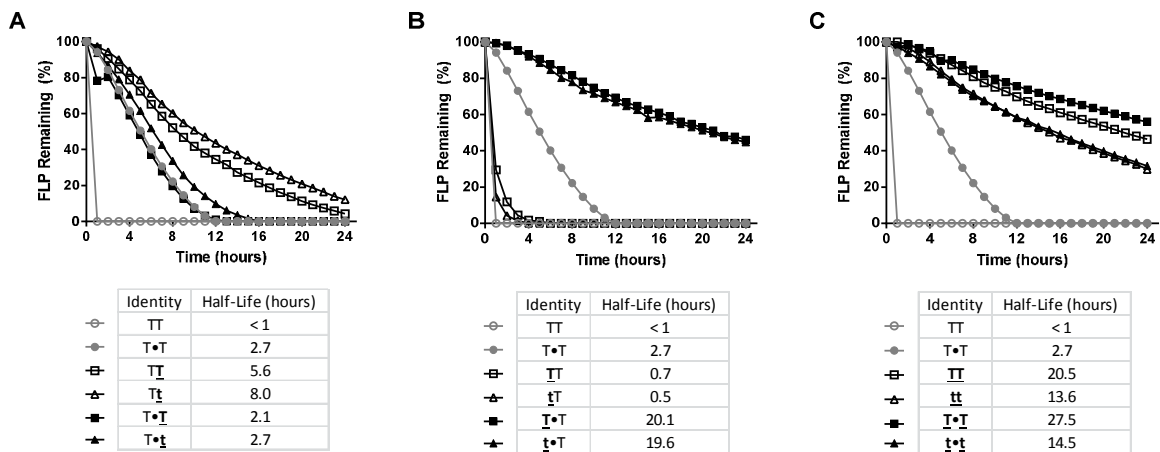

Identity	Half-Life (hours)
TT	< 1
T•T	2.7
T**T**	5.6
T**t**	8.0
T•**T**	2.1
T•**t**	2.7

Identity	Half-Life (hours)
TT	< 1
T•T	2.7
TT	0.7
tT	0.5
T•T	20.1
t•T	19.6

Identity	Half-Life (hours)
TT	< 1
T•T	2.7
TT	20.5
tt	13.6
T•**T**	27.5
t•**t**	14.5

Figure 2. Resistance of GNA-containing oligonucleotides toward degradation by snake venom phosphodiesterase (SVPD) as a function of time. All dT_{20} oligonucleotides were modified by the indicated dinucleotide on the 3'-end which contained a single GNA nucleotide at the 3'-end (A), a single GNA at the penultimate nucleotide (B), or a GNA dinucleotide (C). Uppercase bold underlined and lowercase bold underlined letters indicate (*S*)-GNA and (*R*)-GNA nucleotides, respectively. Phosphorothioate linkages are indicated by the "•" symbol.

X-Ray Crystal Structures of GNA/RNA Heteroduplexes. To better understand the implication of GNA modification on nucleic acid structure in the context of the observed thermal and nucleolytic stability, we used X-ray crystallography to examine how well GNA can be accommodated within an RNA duplex. We determined crystal structures of the self-complementary RNA duplexes 5'-r(CGC*G*AAU)-**T**-(*A*GCG)-3' (SgnT-12-mer; **T**=(*S*)-GNA-T; G:A mismatch italicized), 5'-r(CGC*G*AA[Br]U)-**t**-(*A*GCG)-3' (RgnT-12-mer; [Br]U=5-Br-Uridine; **t**=(*R*)-GNA-T; G:A mismatch italicized), and 5'-r([Br]CGAA)-**T**-(UCG)-3' (SgnT-8-mer, [Br]C=5-Br-Cytidine; **T**=(*S*)-GNA-T) at resolutions of between 1.08 and 1.20 Å (Table S10). All three structures were phased by single-wavelength anomalous dispersion (SAD), using either strontium (SgnT-12-mer) or bromine (RgnT-12-mer, residue U7; SgnT-8-mer, residue C1) as the anomalously scattering ion/atom. Residues are numbered 1 to 12 in the dodecamers and 1 to 8 in the octamer. The asymmetric units of the SgnT-12-mer and -8-mer crystals contain two independent duplexes, whereas a single duplex comprises the asymmetric unit in the RgnT-12-mer crystal.

These structures demonstrate that the GNA nucleotide is accommodated within the RNA duplex in a variety of ways as far as backbone geometry, intra-strand phosphate-phosphate distances, and GNA conformation are concerned (Figure 3). In the SgnT-12-mer duplexes, two of four (*S*)-GNA-T residues per asymmetric unit exhibit twofold disorder, such that together with the two (*R*)-GNA-T residues in the RgnT-12-mer structure and the four (*S*)-GNA-T residues in the SgnT-8-mer structure, there are a total of 10 independent observations for the conformation adopted by a GNA-T and its immediate environment in the three structures. In one of the duplexes in the SgnT-8-mer structure, the GNA-T assumes an *anti* conformation (torsion around the C2'-C3' bond) while the other GNA-T adopts the *syn* conformation (Figure 3B). In the other duplex, the conformations of both GNA residues fall into the *anti* range. Interestingly, the more limited distance that can be spanned by a GNA residue, in comparison to RNA which contains an additional atom in its backbone, leads to a slight intrastrand stretch between phosphate groups 5'-adjacent to the site of the glycol moiety. More or less regular A-type duplex spacing is observed between 3'-adjacent phosphates (Figure 3A). As expected, the *anti* conformation of GNA is associated with a longer distance between 5'- and 3'-intrastrand phosphate groups than a *syn* conformation (Figure 3B), with P···P distances in GNA residues ranging from 4.8 Å to 5.8 Å in the three structures. The slight stretching of the RNA backbone on the 5'-side of the GNA

residue observed in the 8-mer duplex is not as clearly evident in the 12-mer duplexes. These longer duplexes feature a G:A mismatch adjacent to the GNA residue that may also affect backbone geometry. All ribose sugars that bracket GNA-T adopt a C3'-*endo* (North) conformation, with the exception of a single ribose in the SgnT-12-mer that exhibits a C2'-*endo* (South) pucker.
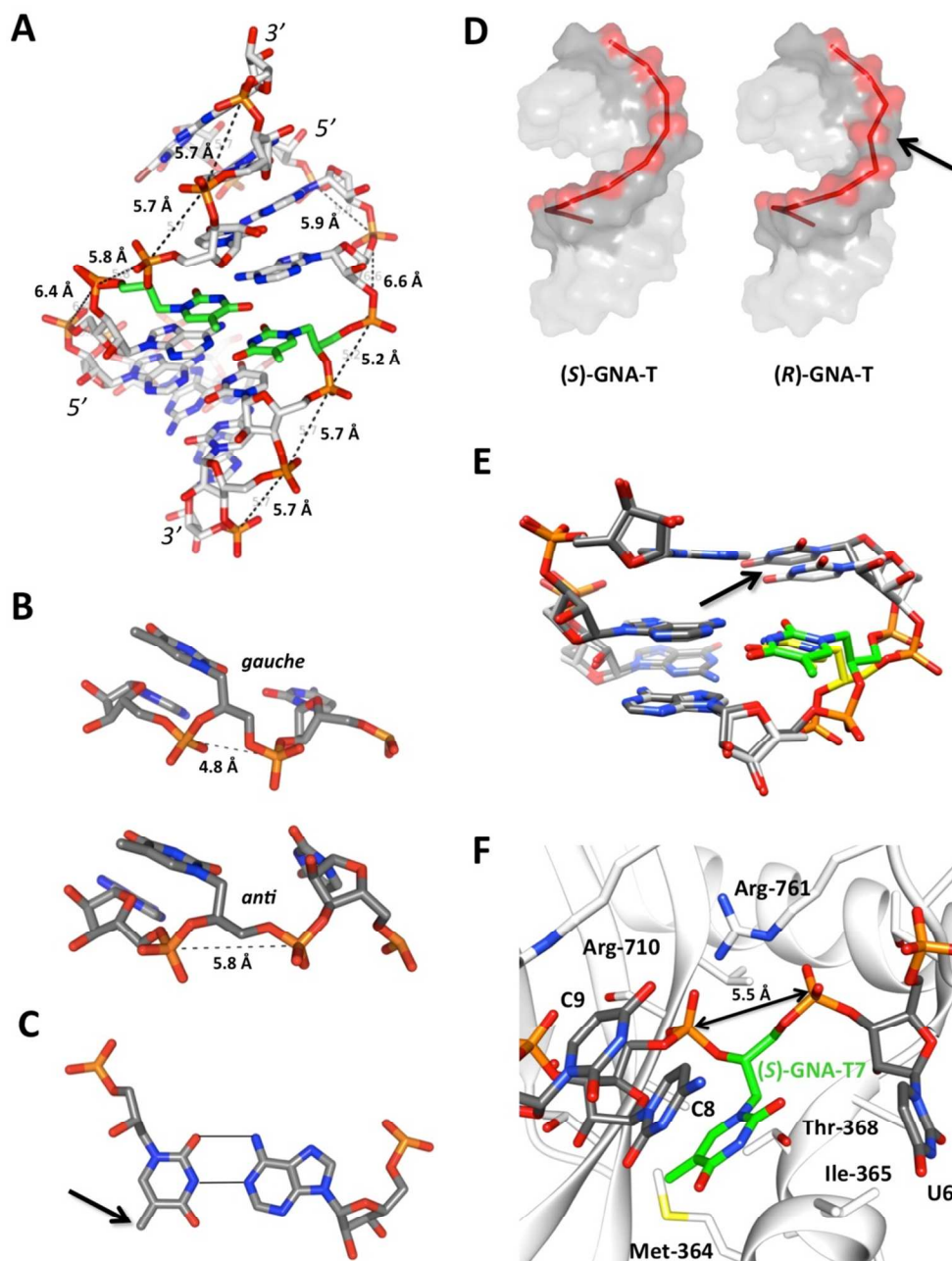
Figure 3. Crystal structures of RNA duplexes modified with both GNA-T stereoisomers. (A) Variations in intrastrand P···P distances in SgnT-8-mer RNA as a consequence of the incorporated GNA-T residues (carbon atoms highlighted in green). (B) GNA nucleotides adopt both *gauche* and *anti* conformations within the structures. (C) Example of an (*S*)-GNA-T:RNA-A base pair showing a rotated nucleobase conformation for the GNA nucleotide (arrow). (D) Global structures of the RNA duplexes incorporating both (*S*)- and (*R*)-isomers of GNA which highlight the phosphate backbones. The two isomers are accommodated differently within the global RNA structure and result in a slight kink in the (*R*)-isomer-containing duplex (arrow). (E)

(*R*)-GNA-T residues distort RNA duplex and pairing geometry to a greater extent than (*S*)-GNA-T residues. Superimposition of A:U and G:A base pairs flanking (*S*)-GNA-T(green):RNA-A and (*R*)-GNA-T(yellow):RNA-A in the two 12-mer duplexes reveals a disruption of the neighboring A:U pair in the (*R*)-GNA-T-modified 12-mer (arrow). (F) An (*S*)-GNA-T residue from the crystal structure of the SgnT-12-mer can seamlessly and with optimal geometry replace an RNA nucleotide at position 7 of the guide strand RNA bound to human Ago 2.[24] The RNA strand assumes a kink at that site that is associated with Ile-365 and results in unstacking of bases of nucleotides 6 and 7.

The most surprising conformational change, a shared feature of all GNA nucleotides in the three structures, is the rotation of the GNA thymine nucleobase such that the C5-methyl group of GNA-T points into the minor groove as opposed to the major groove in a standard Watson-Crick base pair (Figure 3C). For an A:T(U) pair, this change remains without consequence as far as the number of H-bonds (two) are concerned. However, as the thermodynamic data demonstrate, G:C pairs involving GNA residues, unlike A:U pairs, are poorly tolerated in RNA duplexes (Table 1). This difference may possibly be rationalized by the crystallographic data, which would suggest that the rotation of the GNA cytosine base would result in the loss of hydrogen bonding compared to a standard Watson-Crick G:C pair. In order to investigate this further, we paired GNA-C and GNA-G with isoguanosine and isocytidine RNA nucleotides in our 12-mer RNA duplex (Figure 4 and Table 2). Contrary to previous reports[25,26], the RNA duplex containing a central isoC:isoG base pair resulted in a slight destabilization of 2.5 °C. While the incorporation of GNA-C against ribo-G resulted in a destabilization of 16.8 °C, switching the pairing nucleotide to ribo-isoG resulted in a duplex destabilized by only 11.5 °C, representing a 5.3 °C stabilization of the duplex over the GNA-C:G pair. The incorporation of ribo-isoC opposite GNA-G in the duplex had a similar stabilizing effect over the C:GNA-G pair of 1.6 °C. This additional *T*m data strongly supports the hypothesis that, as suggested by the crystal structures, reverse Watson-Crick base pairing is common to GNA pyrimidine nucleotides in RNA duplexes, and helps explain the discrepancy between A:T and G:C base pairs of (*S*)-GNA with RNA.
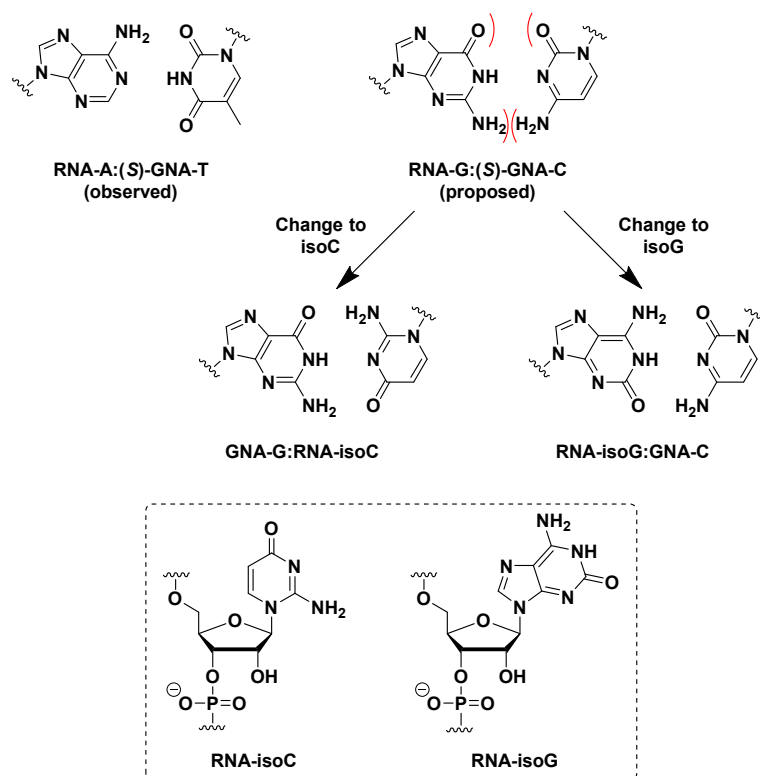
Figure 4. Structures of isocytidine and isoguanosine nucleotides and their potential to form fully complementary base pairs to "rotated" GNA-C or GNA-G.

Table 2. Investigation of (*S*)-GNA crosspairing with isoC and isoG RNA nucleotides.

			5'-UACAGU**X**UAUGU-3' 3'-AUGUCA**Y**AUACA-5'			
X:Y	T_m (°C)	ΔT_m (°C)	**X:Y**	T_m (°C)	ΔT_m (°C)	$\Delta\Delta T_m$ (°C)
C:G	51.2	0.0	isoC:isoG	48.7	-2.5	-
C:isoG	48.5	-2.7	isoC:G	35.8	-15.4[a]	-
C:G	34.4	-16.8	**C**:isoG	39.7	-11.5	**+5.3**
C:**G**	39.2	-12.1	isoC:**G**	40.7	-10.5	**+1.6**

The red indicated RNA nucleotides were substituted as specified in the table. Uppercase bold underlined letters represent (*S*)-GNA nucleotides. All values are the average of two independent measurements at a duplex concentration of 2 µM in 1x PBS buffer (10 mM Na/K phosphate buffer, pH 7.4, with 137 mM NaCl and 2.7 mM KCl). a) The magnitude of destabilization in this base pair has been discussed before.[25]

Comparison of the SgnT- and RgnT-12-mer structures provided insight into the differential destabilization afforded by individual GNA residues when incorporated in RNA duplexes.   A closer look at each of the global duplex structures suggests that the (*R*)-GNA nucleotide introduces a kink within the phosphate backbone, whereas the (*S*)-GNA nucleotide appears to be well accommodated with only minimal distortion (Figure 3D).   The increased backbone distortion caused by the (*R*)-GNA nucleotide is unsurprising considering that the (*R*)-isomer presumably forms a left-handed duplex in contrast to the (*S*)-isomer which has been shown to form a right-handed structure in homo-duplexes of GNA.[20,22,23]   An overlay of base-pair steps adjacent to (*S*)- and (*R*)-GNA-T residues in the two 12-mer duplexes reveals that the latter results in a significant distortion of the 5'-adjacent A:U pair that would be expected to destabilize the duplex (Figure 3E). In general, the structural data support the conclusion that, consistent with the thermal stability data, (*R*)-GNA-T is less well accommodated in an RNA A-form duplex than (*S*)-GNA-T.

***In Vitro* Gene Silencing in Unmodified RNA.** The impact of GNA modification and the influence of C2' stereochemistry on silencing was first assessed within the context of an unmodified siRNA duplex targeting phosphatase and tensin homolog (PTEN) mRNA. Modification of the center of the siRNA duplex with GNA resulted in both nucleobase- and isomer-specific effects (Figure 5).   Whereas GNA-A and GNA-C were tolerated regardless of their absolute configuration, GNA-G and GNA-T showed a strong stereoisomer dependence on inherent potency (Figure 5A).   In the cases where the C2' stereochemistry had an impact on potency, the (*S*)-isomer was roughly 2- or 15-fold more potent than the (*R*)-isomer for G or T substitution, respectively.   We additionally investigated the influence of single GNA base pair incorporation on siRNA potency using the same PTEN sequence (Figure 5B).   The siRNA containing a single (*S*)-GNA-A:T base pair showed activity that was roughly 60-fold greater than the parent. Interestingly, this duplex was almost 10,000-fold more potent that the corresponding duplex containing an (*R*)-GNA base pair.   The C2' configuration did not have a significant impact on the potency of the duplexes containing a GNA-G:C base pair.
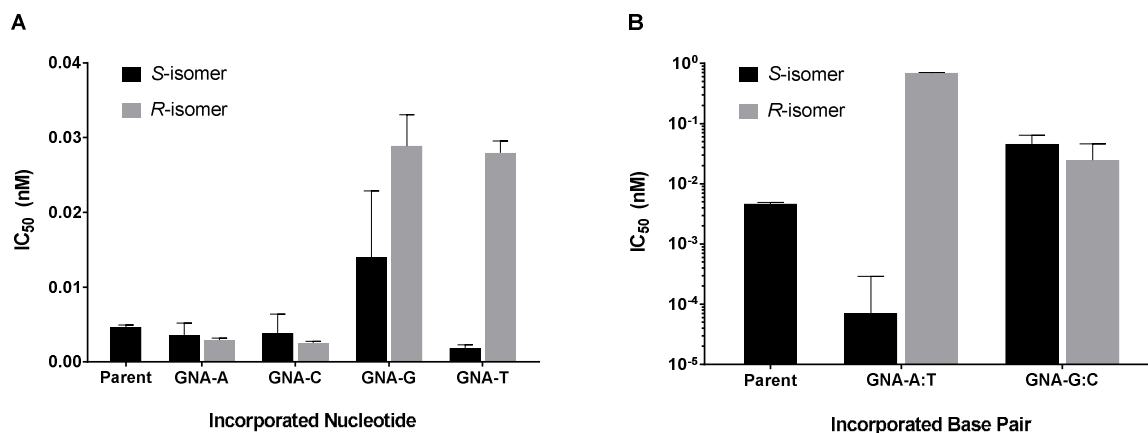
Figure 5. Effect of GNA incorporation on *in vitro* potency of unmodified siRNA targeting PTEN. Either a single nucleotide (panel A) or a single base pair (panel B) in the center of the duplex was substituted as indicated. See Supporting Information for sequence information.

***In Vitro* and *In Vivo* Gene Silencing in Heavily-Modified Conjugate Duplexes.** Based on our initial results which suggested that the (*S*)-isomer of GNA is not only more easily accommodated within the RNA duplex, but also results in, on average, greater potency than the (*R*)-isomer, we only chose to further investigate the (*S*)-isomer within the context of a heavily modified siRNA duplex targeting the rodent transthyretin gene (TTR).[7,27] The parent siRNA, which is fully modified with 2'-OMe, 2'-F, and strategically placed PS modifications, was designed to provide an ideal balance between stability towards nucleolytic degradation and productive association with Ago2.[7,27,28] Since the use of these 2'-modifications results in a high increase of thermal stability, one would presume that additional modification with GNA would still provide a duplex with a higher thermal stability than natural RNA. To determine the positional effect of GNA incorporation on thermal stability and silencing activity, we walked a single (*S*)-GNA nucleotide through both the guide and passenger strand of a 21/23-mer duplex targeting mouse TTR mRNA. The incorporation of (*S*)-GNA led to a variation of thermal stability ranging from +1 °C to -10 °C that was specific to both the position and nature of the nucleobase (see Tables S5 and S6). As expected, the nature of the nucleobase had a large impact on the observed ΔTm values with incorporation of (*S*)-GNA-G or (*S*)-GNA–C being significantly more destabilizing than either (*S*)-GNA-A or (*S*)-GNA–T.

To evaluate the potential of this set of modified duplexes to silence TTR gene expression *in vitro*, a two-dose screen was performed in primary mouse hepatocytes (Figure 6). The incorporation of (*S*)-GNA nucleotides was generally well tolerated in both the guide and passenger strands, with the exception of positions that have been previously shown to be intolerant to modification.[12,18,29] Those positions, 1-2 on the guide strand and 10-12 on the passenger strand, are likely sensitive due to their importance in Ago2 association/loading and sense strand cleavage/removal, respectively.[24,30,31] In addition, loss of potency was observed when GNA was incorporated towards the 3'-end of the guide strand or the 5'-end of the passenger strand, respectively. The loss in silencing activity may have been the result of an improper thermal balancing towards loading of the passenger strand. In contrast, positions 13-15 of the guide and 6-9 of the passenger strand maintained *in vitro* efficacy comparable to the parent. Substitution of positions 3-9 of the guide strand (within the seed region) and positions 13-19 of the passenger strand were also well tolerated. Of particular interest are nucleotides 6-7 of the guide strand where it has been shown that an isoleucine side chain causes a kink in the guide RNA structure complexed with Ago2.[24,30] Modeling an (*S*)-GNA nucleotide in position 7 of the guide strand demonstrated that GNA can efficiently replace the RNA nucleotide with a geometry that appears optimal for interaction with Ago2 (Figure 3F).
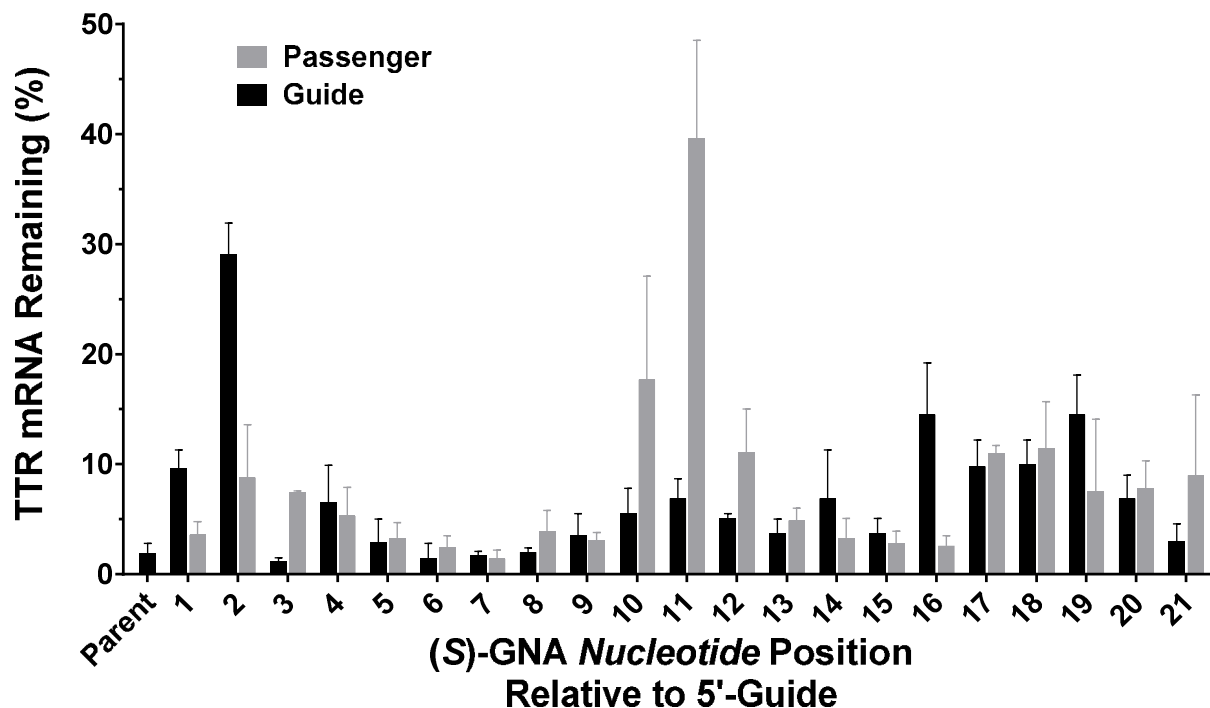
Figure 6. Positional impact of single (*S*)-GNA nucleotide substitution on *in vitro* silencing activity at a concentration of 10 nM siRNA. The nucleotide at the indicated position of the guide or passenger strand was substituted with the corresponding GNA nucleotide. See Table S4 (Supporting Information) for sequence information.

A subsequent study investigated the effect of (*S*)-GNA base pair incorporation within the same TTR siRNA duplex on *in vitro* silencing activity (Figure 7). Although base pair substitution resulted in a loss of activity in many positions, we observed similar trends with respect to the regions where the GNA base pair was tolerated. Those positions were within the seed region of the duplex, mainly at positions 3 and 5-8 relative to the 5'-end of the guide strand.
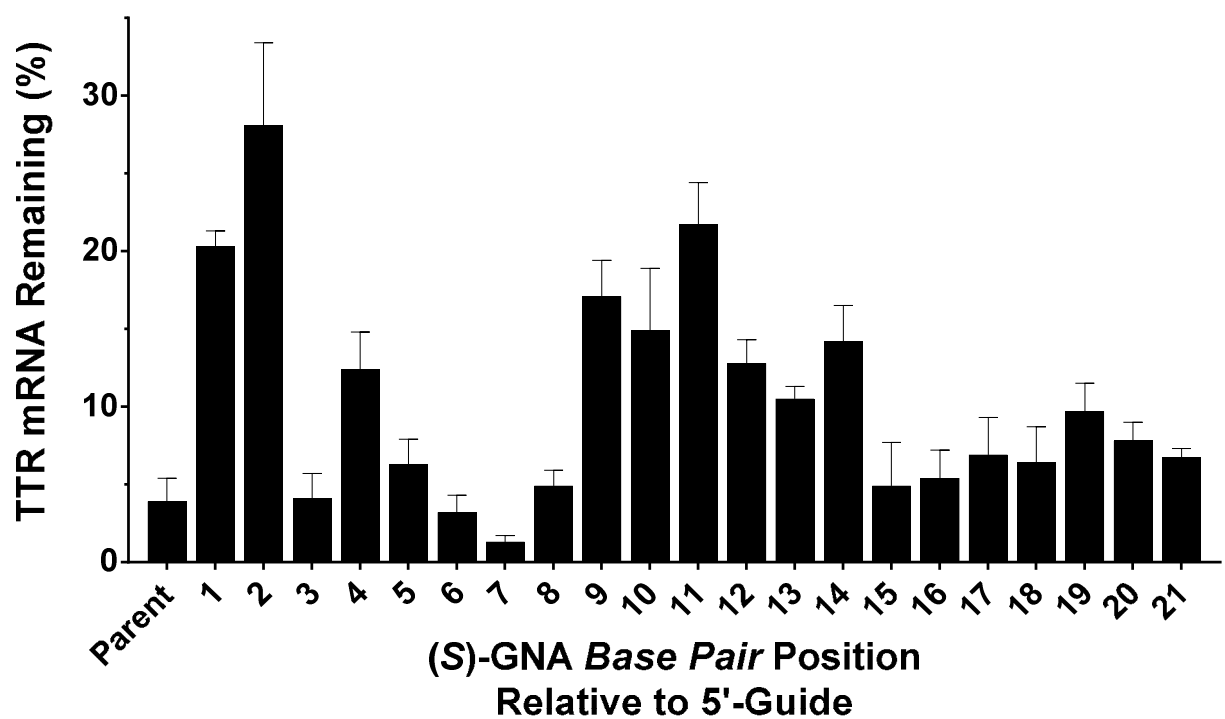
Figure 7. Positional impact of single (*S*)-GNA base pair substitution on *in vitro* silencing activity at a concentration of 10 nM siRNA. The base pair at the indicated position of the guide or passenger strand was substituted with the corresponding GNA base pair. See Table S4 (Supporting Information) for sequence information.

Utilizing several of the siRNA duplexes which were promising in our *in vitro* assays (Table 3), we evaluated the ability of (*S*)-GNA-modified siRNA-GalNAc conjugate duplexes to silence TTR gene expression *in vivo*. After sub-cutaneous administration of each siRNA at a dose of 2.5 mg/kg in mice (approximate ED_{80} of the parent siRNA[7]), both liver mRNA and serum TTR levels were monitored over a period of 21 days (Figure 8). Administration of the parent duplex (**D1**) led to a 77% suppression of TTR mRNA in the liver and an 85% reduction in circulating TTR protein at day 7. The administration of GNA-modified duplexes resulted in similar levels of silencing at day 7 with 84%, 87%, and 84% mRNA suppression for guide (**D2**), passenger (**D3**), and base-pair (**D4**) modified duplexes, respectively (Figure 8A). Knockdown was also reflected in the levels of circulating TTR protein where a reduction of 85%, 84%, and 79% was observed at day 7 for duplexes **D2**, **D3**, and **D4**, respectively (Figure 8B). While the

efficacy of TTR suppression was comparable across the siRNAs, the duration of silencing activity appeared to be somewhat dependent on the placement of the GNA nucleotides. Whereas the duplex modified in the passenger strand with GNA (**D3**) exhibited levels of suppression of TTR mRNA through day 21 comparable to the parent (**D1**), guide (**D2**) and base pair (**D4**) modified duplexes exhibited less durable mRNA knockdown than duplex **D3** (Figure 8A). A similar trend was observed with regards to suppression of the TTR protein. Although the levels of protein suppression between the duplexes differed little at day 21, the passenger modified duplex **D3** (similar to the parent **D1**) showed higher levels of protein suppression on day 14 (approximately 7 days post Nadir) compared to duplex **D4** (Figure 8B).

Table 3. siRNA duplexes targeting rodent TTR.

siRNA duplex	Passenger (5'-3') Guide (3'-5')	T_m (°C)	*In Vitro* IC$_{50}$ (pM)
D1	*A*•a•*CaGuGuUCU*u*GcUcUaUa**A**(L) u•u•u*UgUcAcA*aga*AcGaGaUa*•*U*•u	75.2	20.6 ± 1.9
D2	*A*•a•*CaGuGuUCU*u*GcUcUaUa**A**(L) u•u•u*UgUcAcA*aga*AcG**A**GaUa*•*U*•u	70.9	13.0 ± 1.5
D3	*A*•a•*CaGuGuUCU*u*Gc**T**cUaUa**A**(L) u•u•u*UgUcAcA*aga*AcGaGaUa*•*U*•u	70.3	11.9 ± 1.0
D4	*A*•a•*CaGuGuUCU*u*Gc**T**cUaUa**A**(L) u•u•u*UgUcAcA*aga*AcG**A**GaUa*•*U*•u	66.3	8.1 ± 0.8

Italicized uppercase, lower-case, and uppercase bold underlined letters represent 2'-F, 2'-OMe, and (*S*)-GNA sugar modifications, respectively to Adenosine, Cytosine, Guanosine, and Uridine. (L) represents the tri-N-acetylgalactosamine ligand.[7] Phosphorothioate linkages are indicated by the "•" symbol.
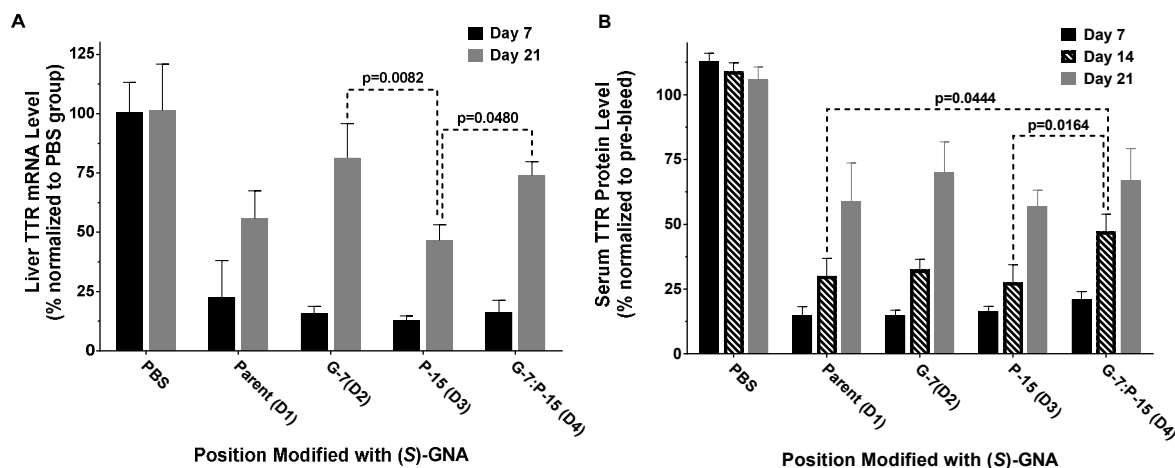
Figure 8. Knockdown of TTR *in vivo* with (*S*)-GNA modified siRNA duplexes dosed at 2.5 mg/kg. Error bars represent the SD from each cohort (n=3). Only those comparisons which are statistically significant are shown in the graph; all others are non-signficant with the exception of all comparisons to PBS which were all significant. (A) TTR mRNA levels measured in the liver. (B) TTR protein levels measured in the serum. G = guide strand, P = Passenger strand.

Discussion

In this study we evaluated the positional effect of GNA on the biophysical and biological properties of siRNA duplexes. As expected, the incorporation of GNA into RNA or RNA-like duplexes led to a significant thermal destabilization. The impact of nucleobase identity on the degree of thermal destabilization may be partially explained via the crystal structures of RNA duplexes containing a single GNA-T nucleotide. If the reverse Watson-Crick pairing mode, a result of a rotated nucleobase, exhibited by the GNA nucleotide in these structures can be extended to the other three nucleobases, it would likely explain the significantly higher degree of destabilization observed for G:C base pairs, where one or more of the three hydrogen bonds of the base pair would be suppressed, vs. A:T base pairs for which the two natural hydrogen bonds of the base pair would be preserved. This observation is supported by thermal melting experiments which show that pairing GNA-C or GNA-G with isoguanosine or isocytidine, respectively, can restore the degree of destabilization back to the level of A and T GNA

nucleotides. The crystal structures additionally demonstrate that the acyclic backbone allows GNA to sample many different backbone conformations within the duplex structure. Of particular interest to siRNA, the model of a GNA nucleotide incorporated in the seed region suggests that GNA's acyclic nature may provide a unique potency benefit by facilitating recognition and cleavage/release of the mRNA target by Ago2.

The potential of any new nucleotide modification incorporated within an siRNA-conjugate duplex will strongly depend on its ability to resist degradation by nucleases. Since chemical modification of an siRNA administered via sub-cutaneous injection is necessary in order to stabilize it against nucleolytic attack along the path to its ultimate destination, modifications which introduce a metabolic instability may negatively impact the efficacy and duration of effect of the corresponding siRNA. Our experiments have shown that GNA has the ability to stabilize linkages against 3'-exonuclease attack in an *in vitro* setting. The ability of a GNA dinucleotide at the 3'-end to create an oligonucleotide highly resistant to exonuclease degradation in the absence of phosphorothioate linkages is especially intriguing.

An increasing body of evidence has demonstrated that the effect of chemical modifications on siRNA duplexes is highly dependent on the specific position within the duplex.[29] Certain sensitive positions typically only tolerate 2'-OH (natural RNA) or 2'-F modifications to maintain RNAi activity.[32] Following this trend, GNA is not well tolerated at positions 1 and 2 of the guide strand or in the central region of the passenger strand. In agreement with previous studies investigating the thermal destabilization of siRNA duplexes, GNA was most well tolerated within the seed region of the duplex. Interestingly, the proposed mechanism of target recognition and cleavage by RISC involves an initial binding of the target mRNA via the seed of the guide strand. Once the mRNA target is recognized, the structure of Ago2 undergoes a shift in which the alpha helix (helix-7) neighboring the guide strand in the seed region is moved away, simultaneously causing a positional shift in the PAZ domain and thereby allowing the guide strand to relax into a near A-form conformation.[31] Of particular relevance to siRNA, the model of a GNA nucleotide incorporated in the seed region suggests that GNA's acyclic nature may provide a potency benefit by facilitating the conformational changes in Ago2 upon recognition and cleavage/release of the mRNA target. Modification with (*S*)-GNA was additionally well tolerated in the 3'-supplemental region (guide positions 12-16) of the duplex; a region proposed to have an additional role in the removal of the sense strand in the

absence of cleavage.[33] For the siRNAs used in this study, the potency improvement of guide-, passenger-, or base-pair modified duplexes observed *in vitro* did not translate into a significant activity benefit *in vivo*. Of the three GNA-modified siRNAs, the passenger modified duplex **D3** performed most similar to the parent *in vivo*, whereas the guide (**D2**) and base-pair (**D4**) modified duplexes trended towards lower potency and duration compared to the parent. The difference in thermal stability observed between these four duplexes may help explain the discrepancy between their *in vitro* and *in vivo* activity. Since the base pair modified duplex **D4** trended towards the lowest *in vivo* activity, but the highest inherent potency *in vitro*, it is possible that the large loss in Tm (8.9 °C) due to the incorporation of the GNA base pair (Table 3) may result in the introduction of metabolic liability into the duplex, while the smaller decrease in Tm observed with **D2** (4.3 °C) and **D3** (4.9 °C) relative to the parent **D1** may not have a large impact on the overall pharmacokinetic profile of those siRNAs.

Conclusions

We have shown that (*S*)-GNA can be utilized as a modification within siRNA, thereby expanding the toolbox of thermally destabilizing modifications.   While both the (*S*)- and (*R*)-isomers were effective towards the suppression of mRNA *in vitro*, we have shown that incorporation of the (*S*)-isomer results in a potency improvement over the (*R*)-isomer. Crystal structures and Tm data of RNA duplexes containing GNA nucleotides indicate that (*R*)-isomer incorporation, preferring a left-handed duplex, resulted in a larger perturbation of the overall duplex structure and thereby a larger thermal destabilization. The *in vitro* and *in vivo* data, along with our modeling studies, demonstrate that GNA is well accommodated in certain positions of the duplex and therefore make GNA an attractive modification for siRNA. It should be noted, however, that in order to be able to consider GNA, or any other novel modification, for therapeutic oligonucleotides, it will need to demonstrate an appropriate preclinical safety profile in rodents along with a substantial (at least 3-fold) pharmacological benefit in higher species. Future work will focus on additional structure-activity and pharmacokinetics studies in order to better understand the *in vivo* translation and to fully harness the potential of GNA within the context of therapeutic siRNAs.

Experimental Section

Synthesis of (S)- and (R)-GNA phosphoramidites. Racemic GNA nucleosides were first synthesized by the groups of Ueda[34] and Imoto[35] and as enantiomerically pure compounds by the group of Holý.[36] The first GNA phosphoramidites and GNA-containing oligonucleotides where synthesized by Cook et. al.[37,38] and Wengel.[39] Meggers and colleagues subsequently published improved and simplified methods for the synthesis of GNA phosphoramidites and GNA oligonucleotides.[19,40,41] To further reduce the total number of synthetic steps for GNA phosphoramidites, we developed a procedure which allows for the ring-opening of enantiopure DMT-glycidol using protected purine nucleobases (Scheme 1). Whereas previous reports mention failure in the direct alkylation of protected purines **3c** and **3d**, we found that the reaction in the presence of *N,N*-diisopropylethylamine resulted in the desired products while preserving the exocylic protecting groups on **3c-3d**. The alkylation of purines **3c** and **3d**, in contrast to alkylation using unprotected purines in the presence of NaH,[40,41] also resulted in the formation of a significant amount of the *N*7 regioisomer which required separation from the *N*9 product via silica gel chromatography. This method could additionally be applied to the pyrimidine nucleobases **3a-3b** resulting in yields similar to previous reports utilizing NaH for deprotonation of the nucleobase. Phosphoramidites of both (*S*)- and (*R*)-isomers of GNA were synthesized from these nucleosides using previously reported procedures.[40,41]
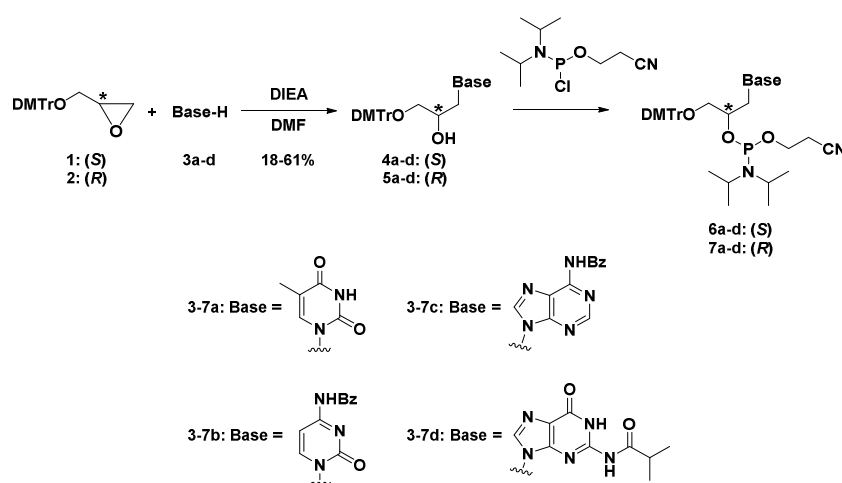
Scheme 1. Procedure for the synthesis of GNA phosphoramidites **6a-6d** and **7a-7d**.

Oligonucleotide synthesis. All oligonucleotides were prepared on an ABI 394 or MerMade 192 synthesizer on a 1 µmole scale using universal or custom supports. All phosphoramidites were used at a concentration of 100 mM in 100% acetonitrile or 9:1 acetonitrile:DMF (2'-OMe-C, 2'-OMe-U, GNA-G) with a standard protocol for 2-cyanoethyl phosphoramidites and ETT activator, except that the coupling time was extended to 400 seconds. Phosphite oxidation to phosphate or sulfurization to phosphorothioate was achieved using a solution of 50 mM I_2 in 9:1 acetonitrile:water or 100 mM DDTT in 9:1 pyridine:acetonitrile, respectively.

MerMade 192 work-up: After the trityl-off synthesis using the MerMade 192, columns were incubated with 150 µL of 40% aqueous methylamine for 30 minutes at room temperature and the solution was drained via vacuum into a 96-well plate. After repeating the incubation and draining with a fresh portion of aqueous methylamine, the plate containing crude oligonucleotides solution was sealed and shaken at room temperature for an additional 60 minutes to completely remove all protecting groups. Precipitation of the crude oligonucleotides was accomplished via the addition of 1.2 mL of 9:1 acetonitrile:EtOH to each well, followed by incubation at -20 °C overnight. The plate was then centrifuged at 3000 RPM for 45 minutes at 4 °C, the supernatant removed from each well, and the pellets resuspended in 950 µL of 20 mM aqueous NaOAc. Each crude solution was finally desalted over a GE Hi-Trap desalting column (Sephadex G25 Superfine) using water to elute the final oligonucleotide products. The identities and purities of all oligonucleotides were confirmed using ESI-MS and IEX HPLC, respectively.

ABI 394 work-up: Standard protocols were used for cleavage and deprotection. Crude oligonucleotides were purified using strong anion exchange and phosphate buffers (pH=8.5) containing sodium bromide. The identities and purities of all oligonucleotides were confirmed using ESI-LC/MS and IEX HPLC, respectively.

Thermal melting experiments. Melting studies were performed in 1 cm path length quartz cells on a Beckman DU800 spectrophotometer equipped with a thermoprogrammer. Each cuvette contained 200 µL of sample solution covered by 125 µL of light mineral oil. Samples were initially annealed in the instrument by heating at a rate of 5 °C/min from 15-95 °C followed by cooling at the same rate from 95-15 °C. After a waiting period of 5 minutes, melting curves were monitored at 260 nm with a heating rate of 1 °C/min from 15-95 °C. Melting temperatures (Tm) were calculated from the first derivatives of the heating curves and the reported values are the result of at least two independent measurements.

Nuclease stability assays. DNA oligonucleotide solutions were prepared at a concentration of 0.1 mg/mL in 50 mM Tris*HCl buffer (pH=8.0), containing 10 mM $MgCl_2$. Snake venom phosphodiesterase I (150 mU/mL) was added to the DNA mixture prior to the first injection and each sample was analyzed for degradation over a time period of 24 hours at room temperature. An analytical sample was removed from the reaction every hour and was eluted (1 mL/min) over a Dionex DNAPac PA200 column (4 x 250 mm, 8 μm particle size) at 30 °C with buffer A (20 mM sodium phosphate buffer, 10% acetonitrile, pH = 11.0) and a linear gradient from 37-52% of buffer B (20 mM sodium phosphate buffer, 1M NaBr, 10% acetonitrile, pH = 11.0) over 10 minutes. Integration of the peak corresponding to the full length product at 260 nm was normalized to the area at time zero and used to calculate the percentage of full length product remaining at each time point. The data points were plotted in Microsoft Excel and first-order decay kinetics were used to determine the half-life, defined as the point where 50% of the full length product was degraded.

Crystallization, X-ray data collection and processing, phasing and refinement. Crystals of SgnT-12-mer were grown by the hanging-drop vapor diffusion technique using the Nucleic Acid Miniscreen (Hampton Research, Aliso Viejo, CA).[42] Droplets (2 μL) containing oligonucleotide (0.6 mM), sodium cacodylate (20 mM, pH=6.0), lithium chloride (20 mM), strontium chloride (40 mM), magnesium chloride (10 mM), spermine tetrahydrochloride (6 mM), and 2-methyl-2,4-pentanediol (MPD; 5% (v/v)) were equilibrated against a reservoir of MPD (1 mL, 35%). RgnT-12-mer crystals were obtained from droplets (2 μL) containing oligonucleotide (0.6 mM), sodium cacodylate (20 mM, pH=6.0), potassium chloride (40 mM), spermine tetrahydrochloride (6 mM), and MPD (5% v/v) that were equilibrated against a reservoir of MPD (1 mL, 35%). SgnT-8-mer crystals were obtained from drops (0.6 μL) containing oligonucleotide (0.5 mM), sodium cacodylate (20 mM, pH=5.5), sodium chloride (40 mM), magnesium chloride (10 mM), hexamine cobalt(III) chloride (10 mM), and MPD (5% v/v) that were equilibrated against a reservoir of MPD (70 μL, 40%). All the crystals were mounted without further cryo-protection and flash-cooled in liquid nitrogen.

X-ray data collection, phasing and refinement. Diffraction data were collected on the 21-ID-F or 21-ID-D beam lines of the Life Sciences Collaborative Access Team (LS-CAT) at the Advanced Photon Source (APS), located at Argonne National Laboratory (Argonne, IL). For

SgnT-12-mer crystals, native data sets were collected on 21-ID-F, but we were not able to phase the structure using molecular replacement. Therefore, anomalous data were collected at 0.769 Å (strontium edge). For RgnT-12-mer crystals the wavelength was tuned to 0.91697 Å (bromine edge) to collect anomalous data. Crystals were kept at 100 K during data collection using a MARCCD 300 detector. Diffraction data were integrated, scaled and merged with HKL2000.[43] A summary of selected crystal data and data collection parameters is provided in Table S10. The structures were phased by the single-wavelength anomalous dispersion (SAD) technique using the program HKL2MAP.[44,45] The resulting experimental electron density maps allowed visualization of all nucleotides in the unit cell (48, SgnT-12-mer; 24, RgnT-12-mer). Building of the models was performed using the program COOT.[46] The initial orientations of the duplex models were optimized by several rounds of rigid body refinement while gradually increasing the resolution of the diffraction data. The refinements were carried out with the program CNS[47], performing simulated annealing, gradient minimization, and refinement of individual isotropic temperature factors. The later refinements were done using the program SHELX[44], keeping aside 5% of the reflections to compute the R-free. After a few cycles of refinement in SHELX, GNA residues were built into the electron density, and the dictionary was adapted and the refinement continued. Ions and water molecules were added on the basis of Fourier $2F_o$-F_c sum and F_o-F_c difference electron density maps, and accepted on the basis of standard distance and B-factor criteria. Final refinements were carried out using anisotropic temperature factors for all nucleic acid and solvent atoms and the final refinement parameters and deviations from ideal geometries are listed in Table S10.

Data from the SgnT-8-mer crystal containing were collected at 100K using the Dectris Eiger 9M detector on the 21-ID-D beamline at LS-CAT tuned to 0.91836 Å (bromine high energy remote). Diffraction data were integrated, scaled and merged with HKL2000.[43] A summary of selected crystal data and data collection parameters is provided in Table S10. The structure was phased by SAD with the program HKL2MAP.[44,45] The resulting experimental electron density maps allowed visualization of all 32 nucleotides in the asymmetric unit. Building of the models was performed using the program COOT.[46] Refinements were carried out using the PHENIX package.[48,49] GNA residues were built into the electron density and refinement continued with a dictionary created using PRODRG.[50] Ions and water molecules were added on the basis of Fourier $2F_o$-F_c sum and F_o-F_c difference electron density maps, and

accepted on the basis of standard distance and B-factor criteria. Final refinements were carried out using anisotropic temperature factors for all nucleic acid and solvent atoms and the final refinement parameters and deviations from ideal geometries are listed in Table S10.

In vitro screening. Primary hepatocytes were obtained from Gibco and cultured in Williams E Medium (Gibco) with 10% fetal bovine serum. Transfection of duplexes was accomplished in a 384-well format, containing 40 µL complete medium, 4.9 µL OptiMem I (Gibco), 0.1 µL RNAiMax (Invitrogen), and 5 µL siRNA. Cells were plated at a density of 5,000 cells per well on collagen-coated plates, and siRNA was added to a final concentration of 10 nM or 0.1 nM. Twenty-four hours after transfection, samples were collected for processing. RNA extraction was performed using Dynabeads (Inivtrogen), followed by reverse transcription according to the manufacturer protocols (ABI, High Capacity). Levels of TTR mRNA were measured after incubation with 10 nM or 0.1 nM siRNA in primary mouse hepatocytes for 24 hours. Mouse TTR was quantified by RT-qPCR (Applied Biosystems # Mm00443267_m1), with mouse GAPDH (4352339E) as loading control. Relative levels of TTR were determined by normalizing to GAPDH RNA expression from the same sample, and these values were subsequently expressed as percent of non-targeting control. All data points are the average of four measurements. The siRNA concentration required to inhibit relative TTR expression by 50% (IC_{50}) was calculated for a subset of the siRNAs by transfecting as described, eight concentrations ranging from 10 nM – 37.5 fM in a six-fold dilution series. IC_{50} values were derived from a 4 parameter fit model with XLFit.

In vivo screening. All studies were conducted using protocols consistent with local, state and federal regulations, as applicable, and approved by the Institutional Animal Care and Use Committee (IACUC) at Alnylam Pharmaceuticals. Animals received a single subscapular subcutaneous injection of 2.5 mg/kg siRNA, prepared as an injection volume of 10 µL/g in PBS. At the indicated time pre- or post-dosing, animals were anesthetized with isofluorane and blood obtained via retroorbital bleed. TTR protein was quantified by ELISA from serum isolated from whole blood. ELISA was performed according to manufacturer protocol (ALPCO, 41-PALMS-E01) after a 3025-fold dilution of the serum samples. Data were normalized to pre-bleed TTR levels. All samples were assayed in duplicate and each data point is the average of all the mice

within each cohort (n=3). Data were analyzed using a two-way ANOVA with a Tukey post-hoc test for multiple comparison in GraphPad Prism.

For evaluation of TTR mRNA in liver, mice were euthanized with carbon dioxide after collection of blood, the liver harvested, and snap-frozen in liquid nitrogen. The liver tissues were processed in a SPEX GenoGrinder, and a small amount powderized tissue transferred to tubes for lysis. RNA extraction was performed with PureLink Pro 96 total RNA Purification Kit (Life Technologies), with RT-qPCR performed as described above. Data were analyzed using a two-way ANOVA with a Tukey post-hoc test for multiple comparisons in GraphPad Prism.

Associated Content

Detailed synthetic procedures, analytical data for oligonucleotides, crystallographic tables, thermal melting data, and *in vitro* screening data. The coordinate files of all structures determined using x-ray crystallography have been deposited in the Protein Data Bank under PDB codes 5V1L, 5V1K, and 5V2H.

Author Information

Corresponding authors: mschlegel@alnylam,com, mmanoharan@alnylam.com

Acknowledgements

References

(1) Elbashir, S. M.; Harborth, J.; Lendeckel, W.; Yalcin, A.; Weber, K.; Tuschl, T. *Nature* **2001**, *411*, 494.
(2) Wang, H.-W.; Noland, C.; Siridechadilok, B.; Taylor, D. W.; Ma, E.; Felderer, K.; Doudna, J. A.; Nogales, E. *Nat. Struct. Mol. Biol.* **2009**, *16*, 1148.

(3) Meister, G.; Landthaler, M.; Patkaniowska, A.; Dorsett, Y.; Teng, G.; Tuschl, T. *Mol. Cell* **2004**, *15*, 185.

(4) Liu, J.; Carmell, M. A.; Rivas, F. V.; Marsden, C. G.; Thomson, J. M.; Song, J.-J.; Hammond, S. M.; Joshua-Tor, L.; Hannon, G. J. *Science* **2004**, *305*, 1437.

(5) Martinez, J.; Patkaniowska, A.; Urlaub, H.; Lührmann, R.; Tuschl, T. *Cell* **2002**, *110*, 563.

(6) Deleavey, G. F.; Watts, J. K.; Damha, M. J. *Current Protocols in Nucleic Acid Chemistry*; Wiley: New York, **2009**; Chapter 16, Unit 16.3.

(7) Nair, J. K.; Willoughby, J. L. S.; Chan, A.; Charisse, K.; Alam, M. R.; Wang, Q.; Hoekstra, M.; Kandasamy, P.; Kel'in, A. V.; Milstein, S.; Taneja, N.; O'Shea, J.; Shaikh, S.; Zhang, L.; van der Sluis, R. J.; Jung, M. E.; Akinc, A.; Hutabarat, R.; Kuchimanchi, S.; Fitzgerald, K.; Zimmermann, T.; van Berkel, T. J. C.; Maier, M. A.; Rajeev, K. G.; Manoharan, M. *J. Am. Chem. Soc.* **2014**, *136*, 16958.

(8) Chan, A.; Liebow, A.; Yasuda, M.; Gan, L.; Racie, T.; Maier, M.; Kuchimanchi, S.; Foster, D.; Milstein, S.; Charisse, K.; Sehgal, A.; Manoharan, M.; Meyers, R.; Fitzgerald, K.; Simon, A.; Desnick, R. J.; Querbes, W. *Mol. Ther.--Nucleic Acids* **2015**, *4*, e263.

(9) Liebow, A.; Li, X.; Racie, T.; Hettinger, J.; Bettencourt, B. R.; Najafian, N.; Haslett, P.; Fitzgerald, K.; Holmes, R. P.; Erbe, D.; Querbes, W.; Knight, J. *J. Am. Soc. Nephrol.* **2017**, *28*, 494.

(10) Fitzgerald, K.; White, S.; Borodovsky, A.; Bettencourt, B. R.; Strahs, A.; Clausen, V.; Wijngaard, P.; Horton, J. D.; Taubel, J.; Brooks, A.; Fernando, C.; Kauffman, R. S.; Kallend, D.; Vaishnaw, A.; Simon, A. *New Engl. J. Med.* **2017**, *376*, 41.

(11) Laursen, M. B.; Pakula, M. M.; Gao, S.; Fluiter, K.; Mook, O. R.; Baas, F.; Langklaer, N.; Wengel, S. L.; Wengel, J.; Kjems, J.; Bramsen, J. B. *Mol. Biosyst.* **2010**, *6*, 862.

(12) Kenski, D. M.; Cooper, A. J.; Li, J. J.; Willingham, A. T.; Haringsma, H. J.; Young, T. A.; Kuklin, N. A.; Jones, J. J.; Cancilla, M. T.; McMasters, D. R.; Mathur, M.; Sachs, A. B.; Flanagan, W. M. *Nucleic Acids Res.* **2010**, *38*, 660.

(13) Kamiya, Y.; Takai, J.; Ito, H.; Murayama, K.; Kashida, H.; Asanuma, H. *ChemBioChem* **2014**, *15*, 2549.

(14) Alagia, A.; Terrazas, M.; Eritja, R. *Molecules* **2015**, *20*, 7602.

(15) Khvorova, A.; Reynolds, A.; Jayasena, S. D. *Cell* **2003**, *115*, 209.

(16) Sano, M.; Sierant, M.; Miyagishi, M.; Nakanishi, M.; Takagi, Y.; Sutou, S. *Nucleic Acids Res.* **2008**, *36*, 5812.

(17) Bramsen, J. B.; Laursen, M. B.; Nielsen, A. F.; Hansen, T. B.; Bus, C.; Langkjær, N.; Babu, B. R.; Højland, T.; Abramov, M.; Van Aerschot, A.; Odadzic, D.; Smicius, R.; Haas, J.; Andree, C.; Barman, J.; Wenska, M.; Srivastava, P.; Zhou, C.; Honcharenko, D.; Hess, S.; Müller, E.; Bobkov, G. V.; Mikhailov, S. N.; Fava, E.; Meyer, T. F.; Chattopadhyaya, J.; Zerial, M.; Engels, J. W.; Herdewijn, P.; Wengel, J.; Kjems, J. *Nucleic Acids Res.* **2009**, *37*, 2867.

(18) Addepalli, H.; Meena; Peng, C. G.; Wang, G.; Fan, Y.; Charisse, K.; Jayaprakash, K. N.; Rajeev, K. G.; Pandey, R. K.; Lavine, G.; Zhang, L.; Jahn-Hofmann, K.; Hadwiger, P.; Manoharan, M.; Maier, M. A. *Nucleic Acids Res.* **2010**, *38*, 7320.

(19) Zhang, L.; Peritz, A.; Meggers, E. *J. Am. Chem. Soc.* **2005**, *127*, 4174.

(20) Schlegel, M. K.; Peritz, A. E.; Kittigowittana, K.; Zhang, L.; Meggers, E. *ChemBioChem* **2007**, *8*, 927.

(21) Schlegel, M. K.; Essen, L.-O.; Meggers, E. *J. Am. Chem. Soc.* **2008**, *130*, 8158.

(22) Schlegel, M. K.; Essen, L.-O.; Meggers, E. *Chem. Comm.* **2010**, *46*, 1094.

(23) Johnson, A. T.; Schlegel, M. K.; Meggers, E.; Essen, L.-O.; Wiest, O. *J. Org. Chem.* **2011**, *76*, 7964.

(24) Elkayam, E.; Kuhn, C.-D.; Tocilj, A.; Haase, Astrid D.; Greene, Emily M.; Hannon, Gregory J.; Joshua-Tor, L. *Cell* **2012**, *150*, 100.

(25) Roberts, C.; Bandaru, R.; Switzer, C. *J. Am. Chem. Soc.* **1997**, *119*, 4640.

(26) Chen, X.; Kierzek, R.; Turner, D. H. *J. Am. Chem. Soc.* **2001**, *123*, 1267.

(27) Allerson, C. R.; Sioufi, N.; Jarres, R.; Prakash, T. P.; Naik, N.; Berdeja, A.; Wanders, L.; Griffey, R. H.; Swayze, E. E.; Bhat, B. *J. Med. Chem.* **2005**, *48*, 901.

(28) Deleavey, Glen F.; Damha, Masad J. *Chem. Biol.* **2012**, *19*, 937.

(29) Kenski, D. M.; Butora, G.; Willingham, A. T.; Cooper, A. J.; Fu, W.; Qi, N.; Soriano, F.; Davies, I. W.; Flanagan, W. M. *Mol. Ther.--Nucleic Acids* **2012**, *1*, e5.

(30) Schirle, N. T.; MacRae, I. J. *Science* **2012**, *336*, 1037.

(31) Schirle, N. T.; Sheu-Gruttadauria, J.; MacRae, I. J. *Science* **2014**, *346*, 608.

(32) Manoharan, M.; Akinc, A.; Pandey, R. K.; Qin, J.; Hadwiger, P.; John, M.; Mills, K.; Charisse, K.; Maier, M. A.; Nechev, L.; Greene, E. M.; Pallan, P. S.; Rozners, E.; Rajeev, K. G.; Egli, M. *Angew. Chem., Int. Ed.* **2011**, *50*, 2284.

(33) Nakanishi, K. *Wiley Interdiscip. Rev.: RNA* **2016**, *7*, 637.

(34) Ueda, N.; Kawabata, T.; Takemoto, K. *J. Heterocycl. Chem.* **1971**, *8*, 827.

(35) Seita, T.; Yamauchi, K.; Kinoshita, M.; Imoto, M. *Makromol. Chem.* **1972**, *154*, 255.

(36) Holý, A.; Ivanova, G. S. *Nucleic Acids Res.* **1974**, *1*, 19.

(37) Cook, P. D.; Acevedo, O. L.; Davis, P. W.; Ecker, D. J.; Hebert, N. Monomeric Diols and Phosphate Linked Oligomers Formed Therefrom. PCT Int. Appl. WO 9518820, **1995**.

(38) Cook, P. D.; Acevedo, O. L.; Davis, P. W.; Ecker, D. J.; Hebert, N. Phospate Linked Oligomers. U.S. Patent 5,886,177, **1999**.

(39) Nielsen, P.; Dreiøe, L. H.; Wengel, J. *Bioorg. Med. Chem.* **1995**, *3*, 19.

(40) Zhang, L.; Peritz, A. E.; Carroll, P. J.; Meggers, E. *Synthesis* **2006**, *2006*, 645.

(41) Schlegel, M. K.; Meggers, E. *J. Org. Chem.* **2009**, *74*, 4615.

(42) Jancarik, J.; Kim, S.-H. *J. Appl. Crystallogr.* **1991**, *24*, 409.

(43) Otwinowski, Z.; Minor, W. *Methods Enzymol.* **1997**, *276*, 307.

(44) Schneider, T. R.; Sheldrick, G. M. *Acta Crystallogr., Section D* **2002**, *58*, 1772.

(45) Pape, T.; Schneider, T. R. *J. Appl. Crystallogr.* **2004**, *37*, 843.

(46) Emsley, P.; Cowtan, K. *Acta Crystallogr., Section D* **2004**, *60*, 2126.

(47) Brunger, A. T.; Adams, P. D.; Clore, G. M.; DeLano, W. L.; Gros, P.; Grosse-Kunstleve, R. W.; Jiang, J.-S.; Kuszewski, J.; Nilges, M.; Pannu, N. S.; Read, R. J.; Rice, L. M.; Simonson, T.; Warren, G. L. *Acta Crystallogr., Section D* **1998**, *54*, 905.

(48) Adams, P. D.; Afonine, P. V.; Bunkoczi, G.; Chen, V. B.; Davis, I. W.; Echols, N.; Headd, J. J.; Hung, L.-W.; Kapral, G. J.; Grosse-Kunstleve, R. W.; McCoy, A. J.; Moriarty, N. W.; Oeffner, R.; Read, R. J.; Richardson, D. C.; Richardson, J. S.; Terwilliger, T. C.; Zwart, P. H. *Acta Crystallogr., Section D* **2010**, *66*, 213.

(49) Afonine, P. V.; Grosse-Kunstleve, R. W.; Echols, N.; Headd, J. J.; Moriarty, N. W.; Mustyakimov, M.; Terwilliger, T. C.; Urzhumtsev, A.; Zwart, P. H.; Adams, P. D. *Acta Crystallogr., Section D* **2012**, *68*, 352.

(50) Schuttelkopf, A. W.; van Aalten, D. M. F. *Acta Crystallogr., Section D* **2004**, *60*, 1355.

Suggestion for Table of Contents Entry